INORGANIC CHEMISTRY FRONTIERS

RESEARCH ARTICLE

View Article Online
View Journal | View Issue

Cite this: *Inorg. Chem. Front.*, 2023, **10**, 4147

A wheel-shaped gallium-sulfide molecular ring with enhanced photocatalytic activity *via* indium alloying†

Tao Wu, *[a,b] Bing Han,[b] Jia-Xin Liu,[a] Jiaxu Zhang,[b] Chaozhuang Xue,[b] Xiang Wang *[c] and Dong-Sheng Li [d]

Received 8th March 2023,
Accepted 27th May 2023

DOI: 10.1039/d3qi00432e

rsc.li/frontiers-inorganic

Wheel-shaped molecular rings are one of the most striking types of molecular aggregates due to their naturally aesthetically appealing architecture, giant size and interesting physical properties and potential applications. Herein, unlike common supertetrahedral cluster-based main-group metal chalcogenides, we report an unprecedented wheel-shaped double-decker $\{Ga_{24}S_{40}\}$ molecular ring (**WSC-1**) with an ~1.6 nm external diameter, which is the first main-group metal sulfide nanoring and the largest ring in the family of inorganic metal sulfide molecular rings. Furthermore, indium was successfully introduced to obtain the first bimetallic main-group metal chalcogenide molecular ring (**WSC-1-In**), exhibiting enhanced photocatalytic dye degradation. This work is of great significance to expand the family of metal chalcogenide molecular rings and demonstrated the great potential of metal chalcogenide molecular rings in the application of photocatalysis.

Introduction

Over the last thirty years, cluster-based crystalline metal chalcogenides (CCMCs),[1,2] combining the porosity and semiconducting features with diverse structures and precisely adjustable compositions, have attracted considerable attention in photo/electro-catalysis,[3–8] ion exchange,[9–11] nonlinear optics[12,13] *etc.* Structurally, as the most important basic building unit in CCMCs, metal chalcogenide clusters with different sizes, shapes, compositions and diversiform assembly modes played a vital role in determining the structure and function of CCMCs.[1,2] Hitherto, the dominant metal chalcogenide clusters assembled in the superlattices of CCMCs are tetrahedrally shaped T*n* (*n* indicates the number of metal layers),[14–16] penta-(P*n*),[17–19] capped-(C*n*),[20–22] super-(T*p*,*q*)[23–27] and TO*n*[28,29] supertetrahedral clusters due to the inherent tetrahedral coordination mode of metal ions (M) in CCMCs and an inflexible Q–M–Q angle in a tetrahedral MQ_4 subunit (Q = S/Se/Te).[1,2] Since metal chalcogenide clusters fundamentally promote the development of CCMCs, it is desirable to synthesize novel non-supertetrahedral clusters with diverse structures and versatile functions to enrich CCMCs with more applications in different fields.

So far, great unremitting efforts have been devoted to the development of non-supertetrahedral CCMCs, including copper-rich open-framework chalcogenides (COCs),[30–34] sphere shaped nano-balls,[35] molecular rings[36–39] and defective atypical supertetrahedral cluster-based chalcogenide frameworks.[40–43] Among these non-supertetrahedral CCMCs, molecular rings deserve attention and research, but limited reports can be found.[36–39] Molecular rings constructed by metal atoms and bridged by pure inorganic O and S/Se anions or O/S/Se atoms of the organic ligands,[44–53] such as cyclic high-nuclear transition-metal compounds,[54,55] have been reported much and have aroused great attention due to their naturally aesthetically appealing architecture and interesting physical properties and potential applications.[52,54,55] So far, only Dai *et al.* reported two kinds of molecular rings based on In–Te/Se clusters which are wheel-shaped $In_{18}Te_{30}$/Se_{30} and triangular $In_{33}Se_{60}$ ring clusters decorated by organic amines[37–39] and Dehnen *et al.* recently reported a

[a]*College of Chemistry and Materials Science, Guangdong Provincial Key Laboratory of Functional Supramolecular Coordination Materials and Applications, Jinan University, Guangzhou, Guangdong 510632, China. E-mail: wutao@jnu.edu.cn*
[b]*College of Chemistry, Chemical Engineering and Materials Science, Soochow University, Suzhou, Jiangsu 215123, China*
[c]*School of New Energy Materials and Chemistry, Leshan Normal University, Leshan, Sichuan 614004, China. E-mail: 516443537@qq.com*
[d]*College of Materials and Chemical Engineering, Hubei Provincial Collaborative Innovation Center for New Energy Microgrid, Key Laboratory of Inorganic Nonmetallic Crystalline and Energy Conversion Materials, China Three Gorges University, Yichang, Hubei 443002, China*

† Electronic supplementary information (ESI) available: Experimental details and additional structural presentations: SCXRD data, EDS, PXRD, TGA, FTIR, additional structural figures, Mott–Schottky plots, UV-vis absorption spectra and additional photocatalytic results (PDF). CCDC 2012952 (**WSC-1**). For ESI and crystallographic data in CIF or other electronic format see DOI: https://doi.org/10.1039/d3qi00432e

square shaped molecular ring constructed by 4 T2 Ge–Se clusters.[56] The slow development of the molecular ring in CCMCs is probably due to the intrinsic tetrahedral coordination mode and inflexible Q–M–Q angle of the MQ_4 subunit (M = In/Ga/Sn/Ge, Q = S/Se/Te),[57,58] and compared with In–Te/Se and Ge–Se molecular rings, creating sulfide based nanorings is much more challenging due to the lower structural flexibility reflected by the relatively rigid S–M–S angle.[37,39]

Herein, we report an unprecedented wheel-shaped Ga–S molecular ring—$[Ga_{24}S_{40}(CPA)_8][(H^+\text{-}CPA)_8(CPA)_8]$ (denoted as **WSC-1**, CPA = cyclopentylamine). Decorated by 8 CPA molecules, **WSC-1** consists of 24 Ga and 40 S atoms, forming a regular double-decker ring structure. Noteworthily, although gallium based molecular wheels built by Ga atoms and bridged organic OMe and OAc ligands have been reported,[47–49] a gallium-sulfide molecular ring has been obtained for the first time and it represents the first example of main-group metal sulfide based nanorings. Besides, **WSC-1** is the largest circular ring cluster in pure metal chalcogenides to date. To adjust the band structure of **WSC-1** for better photocatalytic activity, indium was successfully introduced in a sulfide-based molecular ring for the first time (denoted as **WSC-1-In**) and this first heteronuclear main-group metal chalcogenide molecular ring exhibited enhanced photodegradation of methylene blue (MB) and comparable photocatalytic hydrogen evolution activity.

Experimental

Chemicals

Gallium oxide powder (Ga_2O_3, 99.8%), indium powder (In, 99.99%), sulfur powder (S, 99.9%), cyclopentylamine (CPA, AR, liquid), formamide (AR, liquid), ethanol (AR, liquid), tetraammine platinum(II) nitrate ($Pt(NH_3)_4(NO_3)_2$), and deionized water were all used as supplied without further purification.

Synthesis of WSC-1

Gallium oxide powder (187 mg, 1.00 mmol) and sulfur powder (128 mg, 4.00 mmol) were mixed with cyclopentylamine (4.00 mL) in a 23 mL Teflon-lined stainless steel autoclave and stirred for half an hour. The vessel was then sealed and heated at 190 °C for 7 days and then taken out of the oven. The autoclave was then cooled to room temperature and yellow prism-like crystals (yield: 99.922 mg, 24% based on Ga) were obtained. The raw products were washed three times with ethanol and then dried in air, and the compounds were stable under ambient conditions. Elemental analysis of C, N, and H, found (wt%): C, 28.79; N, 6.80; H, 5.25; calc. (wt%): C, 28.78; N, 6.71; H, 5.47.

Synthesis of In-alloyed WSC-1 (WSC-1-In)

Gallium oxide powder (Ga_2O_3, 112 mg, 0.60 mmol), indium oxide (In_2O_3, 128 mg, 0.46 mmol) and sulfur powder (128 mg, 4.0 mmol) were all mixed with cyclopentylamine (4 mL) in a 23 mL Teflon-lined stainless steel autoclave and stirred for half an hour. The vessel was then sealed and heated at 190 °C for 7 days and then taken out of the oven. Then the autoclave was cooled to room temperature and colorless transparent prism-like crystals (yield: 50.446 mg, 13.3% based on Ga) were obtained. The raw products were washed with ethanol three times and then dried in air, and the compounds were stable under ambient conditions. Elemental analysis of C, N, and H, found (wt%): C, 26.87; N, 6.34; H, 5.37; calc. (wt%): C, 26.85; N, 6.26; H, 5.11.

Methylene blue photodegradation experiments

The photocatalytic activities of the as-synthesized samples and commercial TiO_2 were evaluated from the degradation reaction of Methylene Blue (MB) dye in a glass bottle with a water-cooling system with a 350 W xenon arc lamp as the radiation source. Firstly, 5 mg of each sample was immersed in 20 mL of MB aqueous solution (3.5×10^{-5} M) and stirred for 30 min and then kept still for 10 h in the dark to achieve the adsorption–desorption equilibrium before irradiation. Then, the dispersion was illuminated and stirred under a 350 W xenon arc lamp at ambient temperature. During irradiation, 2 mL solution was sucked up from the reaction reactor at every specific interval and centrifuged at 8000 rpm for 3 minutes. The resulting supernatant was analyzed on a UV-Vis spectrophotometer (UV2450, Shimadzu). The degradation efficiency was reported as C_t/C_0, where C_t is each irradiated time interval and C_0 is the initial equilibrium concentration of MB according to the main peak of absorption. After the reaction, the mixture was filtered and the powder was collected for the powder X-ray diffraction (PXRD) test.

Results and discussion

Crystal structure

Pale-yellow prismatic crystals of **WSC-1** were synthesized *via* the solvothermal reaction of Ga_2O_3 and S powder in the mixed solvents of CPA and deionized water at 190 °C for 7 days (Fig. S1a†). Single-crystal X-ray diffraction (SCXRD) analysis revealed that **WSC-1** crystallizes in a tetragonal system with the space group of $I\bar{4}$ (Table S1†) and represents a unique wheel-shaped molecular ring (Fig. 1), while the charge balancing counter ions and solvent molecules could not be completely located due to significant disorder. Notably, CPA is essential for the crystallization of **WSC-1** since no crystals were obtained when replaced by other cycloamines such as DACH (1,2-diaminocyclohexane), the one used in In–Te/Se molecular rings.[37,39] According to the charge balance rule, C/H/N elemental analysis (EA) and energy-dispersive spectroscopy (EDS) measurements (Fig. S2†), the empirical formula of **WSC-1** was determined to be $[Ga_{24}S_{40}(C_5H_{11}N)_{16}(C_5H_{12}N)_8]$ (cationic $C_5H_{12}N$ stands for protonated CPA). **WSC-1** was also characterized by thermogravimetric analysis (TGA) and Fourier transform infrared (FTIR) spectroscopy (Fig. S3a and S4†) and the experimental powder X-ray diffraction (PXRD) pattern of the as-synthesized **WSC-1** confirmed its phase purity (Fig. S5a†).

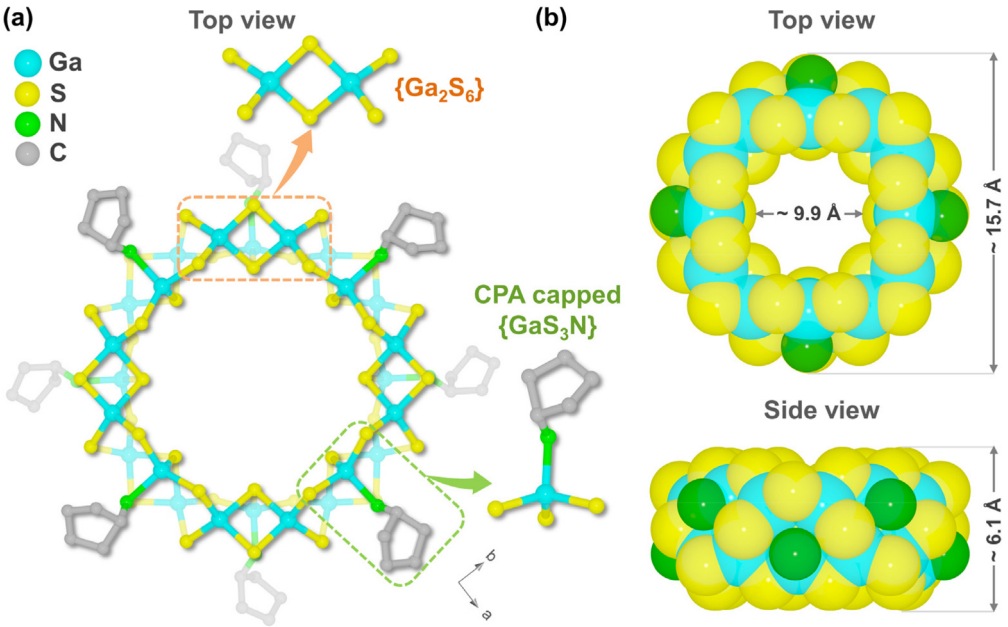

Fig. 1 View of the structure of the **WSC-1** molecular ring in (a) ball-stick and (b) space-filling modes. All H and some C atoms are omitted for clarity.

As shown in Fig. 1a, **WSC-1** comprises a wheel-shaped anion $[Ga_{24}S_{40}(CPA)_8]^{8-}$, where eight CPA molecules are mono-capped with eight Ga atoms and are located alternately above and below the outer side of the wheel. In this ring, all 24 Ga^{3+} sites are tetrahedrally coordinated while there are two types of coordination modes of S^{2-} (μ_2-S^{2-} and μ_3-S^{2-}). Structurally, $[Ga_{24}S_{40}(CPA)_8]^{8-}$ is constructed by eight $\{Ga_2S_6\}$ units alternately interlinked with eight CPA mono-coordinated $\{GaS_3N\}$ tetrahedra through sharing the adjacent vertex μ_2/μ_3-S^{2-} (Fig. 1a and S6†). Each $\{Ga_2S_6\}$ building unit is 5-connected with three $\{GaS_3N\}$ tetrahedra and two other $\{Ga_2S_6\}$ units while each $\{GaS_3N\}$ unit is capped by three $\{Ga_2S_6\}$ units and one CPA molecule (Fig. S7†).

On the other hand, **WSC-1** can also be viewed as a double-decker ring with a 'two-stranded' topology with respect to Ga atoms and the two $[Ga_{12}]$ folded quasi-ideal squares (coordinated CPA is omitted) are mirror symmetric by twisting ~45°, linking together through 8 μ_2-S^{2-} and 8 μ_3-S^{2-} (Fig. 2a). In each $[Ga_{12}]$ unit, 3 Ga^{3+} ions and 4 adjacent bridged μ_2-S^{2-} are alternately arranged approximately in a 1D polymeric chain of *ca.* 10.98 Å and such 4 chains connected end-to-end by sharing an S^{2-} ion to form a folded quasi-ideal square (Fig. 2b). This structure is analogous to the reported In–Te nanoring. Besides, the **WSC-1** ring shows a pseudo-C_{4v} symmetry, but it is an accurate C_4 point group when considering the eight decorated CPA molecules. It is reported that the small molecules or ions located at the center of the ring can act as important templates in the formation of ring structures and we also found peaks of residual electron density at the center of the ring from the Fourier electron density map, which are believed to act as key templates to shape this wheel-like molecular ring.[37,39] However, these peaks cannot be well resolved due to serious disorder, and hence removed by SQUEEZE in SCXRD data refinement.

The bond length of Ga–S and bond angles of S–Ga–S of **WSC-1** are in the range of 2.203(4)–2.378(5) Å and 94.72(15)–115.27(16)°, respectively (Tables S2 and S3†), while for Ga1 and Ga4 in the asymmetric unit (Fig. S8†), the Ga–N distances are 2.053(12) and 1.98(4) Å, and the bond angles of N–Ga–S range from 102.3(3) to 110.7(4)°. All the above values are consistent with those in literature reports.[59–61] Provided by space-filling models (Fig. 1b), the average central hole and external diameter and thickness of the molecular ring are *ca.* 9.92 Å, 15.72 Å and 6.06 Å (estimated from the distance of two opposite S atoms without considering van der Waals radii), respectively, demonstrating that **WSC-1** is the largest standard molecular ring ever found in pure metal chalcogenides (Table S4†).

As shown in Fig. 3, the anion rings of **WSC-1** stacked parallel to each other and packed together to form a staggered pseudo-supramolecular nanotubular architecture along the *c* direction, where the distance between two adjacent rings is ~6.6 Å in the *c* direction, while the adjacent nanotubes are ~13.2 Å apart in the *a* or *b* direction and separated by ~4.7 Å along the [110] direction. Moreover, by connecting the barycenter of the adjacent cluster, the arrangement mode of rings is a squashed BCU (body centered cubic)-type superlattice (Fig. S9†).

The solvent-accessible void space of **WSC-1** is only 56.0% as calculated using PLATON software, which is not outstanding in discrete CCMCs (Table S5†), indicating that it is insoluble in common solvents such as water due to strong cation–anion electrostatic interactions and van der Waals forces between clusters and protonated organic amines. This is like other known closely packed discrete CCMCs and different from the thermodynamic unstable CCMCs constructed by loosely packed discrete clusters.[6,62–66]

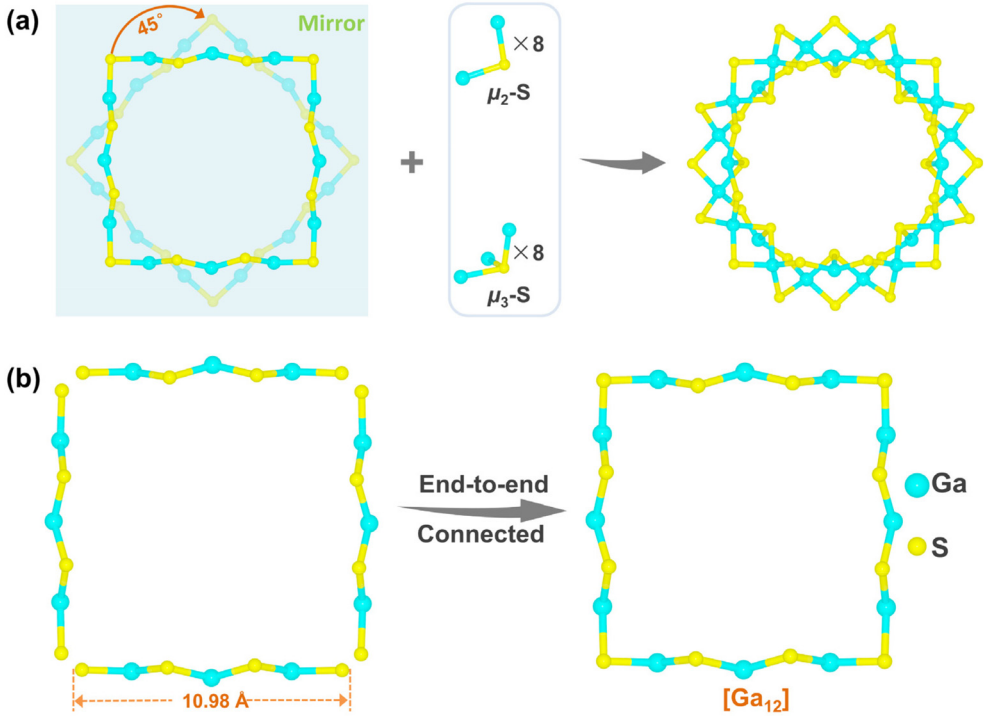

Fig. 2 (a) Mirror symmetric two [Ga_{12}] folded quasi-ideal square (coordinated CPA is omitted) linked together through 8 μ_2-S^{2-} and 8 μ_3-S^{2-} by twisting ~45° to form the wheel-shaped molecular ring and (b) a [Ga_{12}] unit constructed by 4 1D polymeric chains of 3 Ga^{3+} ions and 4 adjacent bridged μ_2-S^{2-}.

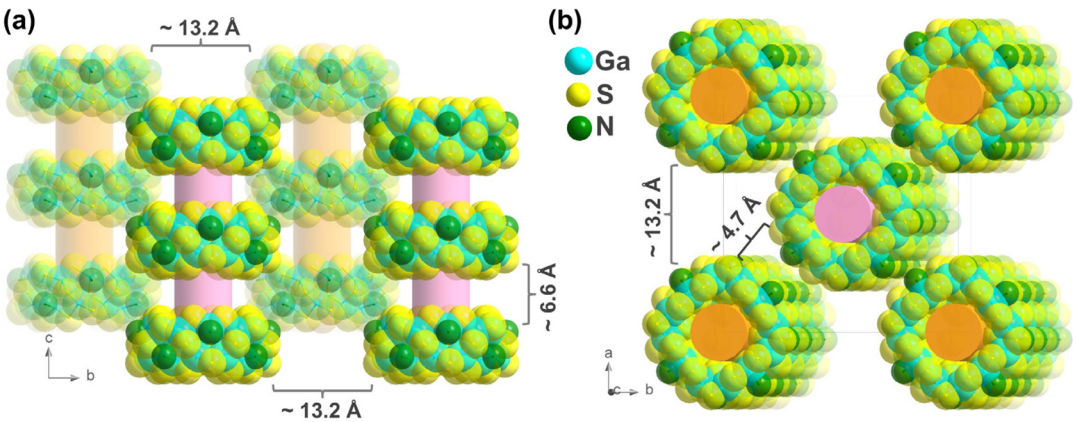

Fig. 3 Packing diagrams of **WSC-1** molecular rings viewed along (a) the *a* axis and (b) *c* axis showing different alternations of adjacent pseudo-supramolecular nanotubes (emphasized with disparate colors). H and C atoms are omitted for clarity.

Indium alloying, optoelectronic properties and photocatalytic activities

As alloying is an effective strategy to modulate the bandgap sizes and optical- and electronic-related properties of CCMCs for better photocatalytic activity,[19,34,65] indium alloyed **WSC-1** (denoted as **WSC-1-In**) was successfully prepared (Fig. S1b†). As the introduced In atoms could theoretically appear at every tetrahedral metal site of the cluster since In and Ga are in the same main group with equivalent valence states and the SCXRD data match the statistical result, it is difficult to find defined Ga or In positions for every metal site in the cluster which could be occupied in a mixed way by Ga and In.[19,34] Nonetheless, an In/Ga ratio of 0.491 (*ca.* 7.9 per 24 metal atoms in one molecular ring) could be determined for **WSC-1-In** crystals by inductively coupled plasma atomic emission spectrometry (ICP-AES) analysis, which is close to the energy-dispersive spectroscopy (EDS) results (Fig. S10†). The corresponding elemental mapping (Fig. S11†) pictures demonstrated that indium is evenly distributed in **WSC-1** crystals. Besides,

the PXRD pattern of **WSC-1-In** matches well with that of **WSC-1** (Fig. S5b†), indicating that **WSC-1-In** is isostructural. In addition, both **WSC-1** and **WSC-1-In** were stable in open air for at least 6 months (Fig. S12†).

Solid-state UV-vis diffuse reflectance (DRS) spectroscopy and Mott–Schottky (MS) measurements were firstly performed to determine the band structures of the title compounds. As depicted in Fig. 4a, from the extrapolation of linear regions of Tauc plots, the band gaps of **WSC-1** and **WSC-1-In** are *ca.* 3.79 eV and 3.83 eV, respectively, consistent with their different colors (Fig. S1†). Beside the optical absorption capability, the positive slopes of MS plots in Fig. 4b and Fig. S13† indicate that both **WSC-1** and **WSC-1-In** are n-type semiconductors.[6,67,68] From the MS plots, the flat-band potential (E_F) of **WSC-1** and **WSC-1-In** is found to be −0.8 V and −1.01 (*vs.* NHE, pH = 7), respectively, where the conduction band (CB) potential (E_{CB}) can be estimated to be −0.9 V and −1.11 V *via* the equation $E_{CB} = E_F - 0.1$ for an n-type semiconductor.[6,8,67,68] In combination with the measured band gaps from DRS, the calculated valence band potentials of **WSC-1** and **WSC-1-In** are 2.89 V and 2.72 V (*vs.* NHE, pH = 7), respectively. Meanwhile, as low recombination rates of photo-induced electron–hole pairs are conducive to photocatalysis, photoelectric response and electrochemical impedance spectroscopy (EIS) measurements were, therefore, performed to explore the effect of In-alloying on the separation efficiency of charge carries.[6,8,65] As shown in Fig. 4c, both **WSC-1** and **WSC-1-In** exhibited rapid responses upon illumination and good reproducibility during the light on–off mode, and the photocurrent density of **WSC-1-In** (~0.96 μA cm^{-2}) is *ca.* 2-fold larger than that of **WSC-1** (~0.47 μA cm^{-2}). Besides, **WSC-1-In** displayed a smaller arc radius than **WSC-1** in the Nyquist plots (Fig. 4d). The above results indicate the suppressed charge recombination and superior conductivity of **WSC-1-In** compared to those of **WSC-1**, consistent with previous research studies that In-alloying could facilitate electron transport in CCMCs.[19,34]

Given their different band structures and optoelectronic features, we further investigated their performance in dye photodegradation and photocatalytic H_2 evolution. As shown in Fig. S14a,† the blank experiment shows that the characteristic absorption peak of MB remains almost constant for 13 min without any catalysts, suggesting negligible photo-induced self-decomposition. Conversely, the absorbance of MB rapidly decreases over illumination time when **WSC-1**, **WSC-1-In** and commercial TiO_2 are used as catalysts (Fig. 5a, b and Fig. S14b†). As displayed in Fig. 5c, **WSC-1-In** exhibits the best photocatalytic performance among all catalysts as 98.1% of MB was decomposed within 5 min, whereas only 58.2% MB and 33.8% MB were degraded within the same time for **WSC-1** and commercial TiO_2. Assuming that the dye degradation is a pseudo-first-order reaction,[10,34,69–72] the apparent rate constant (K_a) was calculated to be 0.8144 min^{-1} for **WSC-1-In**, which is *ca.* 4 times faster than that of **WSC-1** (K_a = 0.2000 min^{-1}) (Fig. 5d).

As the indirect dye photosensitization degradation or self-sensitized degradation usually occurred during the degradation process,[73,74] it should be excluded in this experiment. According to the literature,[75] the redox potential of MB is +0.05 V (*vs.* NHE, pH = 7), which is much more positive than the CB potential of **WSC-1-In** (−1.11 eV *vs.* NHE, pH = 7). As a

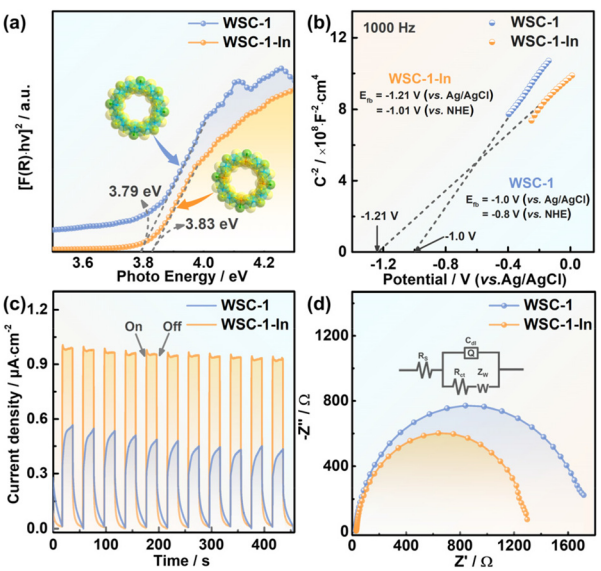

Fig. 4 (a) Tauc plots of **WSC-1** and **WSC-1-In** derived from solid-state UV-Vis diffuse reflectance spectra; (b) Mott–Schottky plots of **WSC-1** and **WSC-1-In** measured at a frequency of 1000 Hz; (c) photocurrent response curves of **WSC-1** and **WSC-1-In** under a 0.4 V bias potential; and (d) Nyquist plots of impedance measured from **WSC-1** and **WSC-1-In** (inset is the fitted equivalent circuit model).

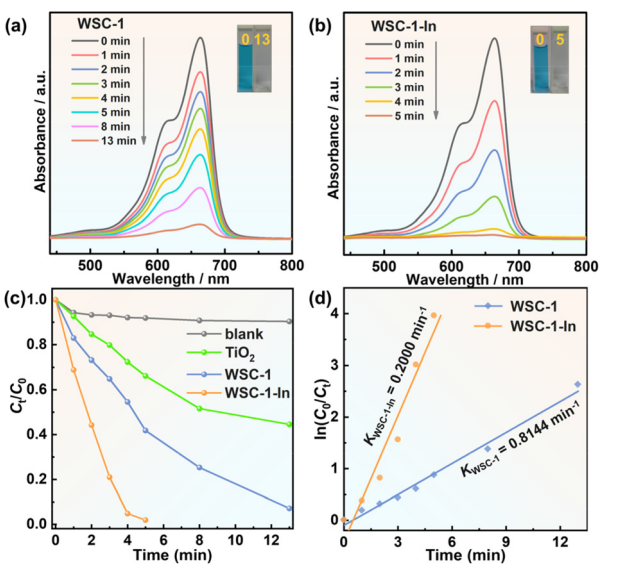

Fig. 5 UV-Vis absorption spectra of MB *versus* time with (a) **WSC-1** and (b) **WSC-1-In** as catalysts under full spectrum solar light irradiation; (c) photodegradation efficiency curves of different catalysts with the blank as the control; and (d) linear plots of ln(C_0/C_t) over time for the photocatalytic degradation of MB.

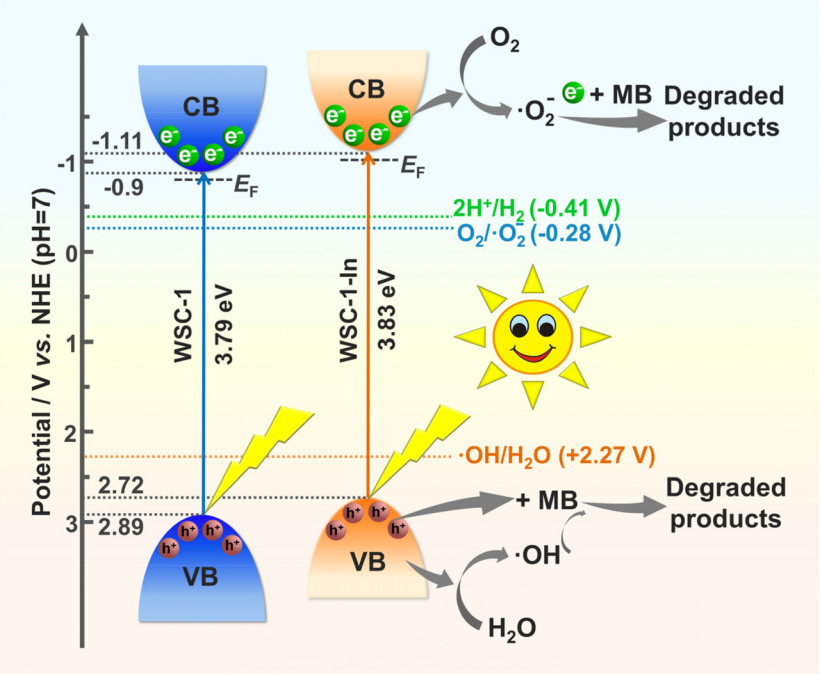

Fig. 6 Schematic illustration of the energy band diagrams of **WSC-1** and **WSC-1-In** and the possible electron and hole transfer mechanism upon solar light illumination.

result, the photo-induced electrons originating from MB molecules cannot transfer to the CB of **WSC-1-In**; hence it could be inferred that there would be no dye-sensitive effect during the degradation process. Consequently, such superior photocatalytic activity should be related to the suitable band structure and high charge carrier separation efficiency of **WSC-1-In** as demonstrated above.[6,8,65,69,71]

The correlative degradation mechanism proposed for the photocatalytic degradation of MB is based on the known band structure as illustrated in Fig. 6. **WSC-1-In** is taken as an example, as its CB potential is negative compared to $E^\circ(O_2/^\bullet O^-_2)$ (−0.28 V *vs.* NHE, pH = 7); when irradiated with solar light, the electrons underwent excitation from the valence band (VB) to the CB. According to literature reports,[8,70,71] the excited photoelectrons are captured by the chemically adsorbed O_2 molecules on the surface to yield the superoxide radical $^\bullet O^-_2$, which further participates in the degradation of dye molecules. On the other hand, its VB potential is positive compared to $E^\circ(^\bullet OH/H_2O)$ (+2.27 V *vs.* NHE, pH = 7), and the remaining photogenerated holes oxidize H_2O molecules to yield reactive $^\bullet OH$ species. These radicals are reactive species contributing to the degradation of MB to H_2O and CO_2 as the final products. Although the band gap of **WSC-1-In** is slightly larger than that of **WSC-1** (Fig. 4a), its CB is more negative, which is more favourable for the formation of $^\bullet O^-_2$ with high oxidative ability. Thus, the photocatalytic activity of In-alloyed **WSC-1-In** is significantly higher than that of **WSC-1**. As photogenerated electrons worked with holes to promote photocatalytic oxidation during the photocatalytic process, the photodegadation efficiency of **WSC-1-In** and **WSC-1** is greatly enhanced, making them among the most active cluster-based metal chalcogenides for photocatalytic dye degradation (Table S6†). Noticeably, the title compounds are stable and retain their original crystallinity after photodegradation (Fig. S15†), yet the crystallinity of **WSC-1** and **WSC-1-In** was destroyed after two runs of photodegradation (results not shown in this study), probably because of the quite common photocorrosion in sulfide based photocatalysts.[76] Moreover, the H_2 generation rate of **WSC-1-In** (~22.82 μmol h^{-1} g^{-1}) is *ca.* 3.4 faster than that of **WSC-1** (6.71 μmol h^{-1} g^{-1}) (Fig. S16†), which is consistent with the dye photodegradation results.

Conclusions

In summary, different from the usual supertetrahedral clusters, a unique wheel-shaped double-decker inorganic gallium-sulfide molecular ring (**WSC-1**) with an external diameter of ~1.6 nm is reported here, representing the first case of a main-group metal sulfide nanoring and the largest standard ring in pure metal chalcogenides thus far. The introduction of indium to **WSC-1** makes the heteronuclear molecular ring (**WSC-1-In**) exhibit highly efficient photocatalytic dye degradation toward MB and comparable photocatalytic H_2 evolution related to a modulated suitable band structure and enhanced photogenerated carrier separation efficiency. This work revealed the great potential of a new generation of large-sized inorganic metal chalcogenide molecular rings with tunable properties in the application of photocatalysis.

Author contributions

Tao Wu: funding acquisition, project administration, resources, and supervision. Bin Han: data curation, formal analysis, investigation, methodology, and validation. Jia-Xin Liu: investigation. Jiaxu Zhang: formal analysis. Chaozhuang Xue: formal analysis. Xiang Wang: conceptualization, data curation, formal analysis, investigation, methodology, writing – reviewing and editing, and supervision. Dong-Sheng Li: funding acquisition.

Conflicts of interest

There are no conflicts to declare.

Acknowledgements

We acknowledge the National Natural Science Foundation of China (92261205 and 22071165) and the 111 Project (D20015).

References

1 J. Zhang, X. Bu, P. Feng and T. Wu, Metal Chalcogenide Supertetrahedral Clusters: Synthetic Control over Assembly, Dispersibility, and Their Functional Applications, *Acc. Chem. Res.*, 2020, **53**, 2261–2272.

2 J. Zhang, P. Feng, X. Bu and T. Wu, Atomically Precise Metal Chalcogenide Supertetrahedral Clusters: Frameworks to Molecules, and Structure to Function, *Natl. Sci. Rev.*, 2021, **9**, nwab076.

3 W. Wang, X. Wang, D. Hu, H. Yang, C. Xue, Z. Lin and T. Wu, An Unusual Metal Chalcogenide Zeolitic Framework Built from the Extended Spiro-5 Units with Supertetrahedral Clusters as Nodes, *Inorg. Chem.*, 2018, **57**, 921–925.

4 J. Lv, J. Zhang, C. Xue, D. Hu, X. Wang, D.-S. Li and T. Wu, Two Penta-Supertetrahedral Cluster-Based Chalcogenide Open Frameworks: Effect of the Cluster Spatial Connectivity on the Electron-Transport Efficiency, *Inorg. Chem.*, 2019, **58**, 3582–3585.

5 J. Zhang, X. Wang, J. Lv, D.-S. Li and T. Wu, A Multivalent Mixed-Metal Strategy for Single-Cu^{+}-Ion-Bridged Cluster-Based Chalcogenide Open Frameworks for Sensitive Nonenzymatic Detection of Glucose, *Chem. Commun.*, 2019, **55**, 6357–6360.

6 M. Hao, Q. Hu, Y. Zhang, M. Luo, Y. Wang, B. Hu, J. Li and X. Huang, Soluble Supertetrahedral Chalcogenido T4 Clusters: High Stability and Enhanced Hydrogen Evolution Activities, *Inorg. Chem.*, 2019, **58**, 5126–5133.

7 D. Hu, X. Wang, X. Chen, Y. Wang, A. N. Hong, J. Zhong, X. Bu, P. Feng and T. Wu, S-Doped $Ni(OH)_2$ Nano-Electrocatalyst Confined in Semiconductor Zeolite with Enhanced Oxygen Evolution Activity, *J. Mater. Chem. A*, 2020, **8**, 11255–11260.

8 Y. Wang, Z. Zhu, Z. Sun, Q. Hu, J. Li, J. Jiang and X. Huang, Discrete Supertetrahedral T5 Selenide Clusters and Their Se/S Solid Solutions: Ionic-Liquid-Assisted Precursor Route Syntheses and Photocatalytic Properties, *Chem. – Eur. J.*, 2020, **26**, 1624–1632.

9 H. Yang, M. Luo, L. Luo, H. Wang, D. Hu, J. Lin, X. Wang, Y. Wang, S. Wang, X. Bu, P. Feng and T. Wu, Highly Selective and Rapid Uptake of Radionuclide Cesium Based on Robust Zeolitic Chalcogenide Via Stepwise Ion-Exchange Strategy, *Chem. Mater.*, 2016, **28**, 8774–8780.

10 X. Chen, X. Bu, Q. Lin, C. Mao, Q.-G. Zhai, Y. Wang and P. Feng, Selective Ion Exchange and Photocatalysis by Zeolite-Like Semiconducting Chalcogenide, *Chem. – Eur. J.*, 2017, **23**, 11913–11919.

11 M.-L. Feng, D. Sarma, Y.-J. Gao, X.-H. Qi, W.-A. Li, X.-Y. Huang and M. G. Kanatzidis, Efficient Removal of $[UO_2]^{2+}$, Cs^{+}, and Sr^{2+} Ions by Radiation-Resistant Gallium Thioantimonates, *J. Am. Chem. Soc.*, 2018, **140**, 11133–11140.

12 N. W. Rosemann, J. P. Eußner, A. Beyer, S. W. Koch, K. Volz, S. Dehnen and S. Chatterjee, A Highly Efficient Directional Molecular White-Light Emitter Driven by a Continuous-Wave Laser Diode, *Science*, 2016, **352**, 1301–1304.

13 B.-W. Liu, X.-M. Jiang, H.-Y. Zeng and G.-C. Guo, $[ABa_2Cl][Ga_4S_8]$ (A = Rb, Cs): Wide-Spectrum Nonlinear Optical Materials Obtained by Polycation-Substitution-Induced Nonlinear Optical (NlO)-Functional Motif Ordering, *J. Am. Chem. Soc.*, 2020, **142**, 10641–10645.

14 G. Férey, Supertetrahedra in Sulfides: Matter against Mathematical Series?, *Angew. Chem., Int. Ed.*, 2003, **42**, 2576–2579.

15 X. Xu, W. Wang, D. Liu, D. Hu, T. Wu, X. Bu and P. Feng, Pushing up the Size Limit of Metal Chalcogenide Supertetrahedral Nanocluster, *J. Am. Chem. Soc.*, 2018, **140**, 888–891.

16 D.-D. Yang, W. Li, W.-W. Xiong, J.-R. Li and X.-Y. Huang, Ionothermal Synthesis of Discrete Supertetrahedral Tn (n = 4, 5) Clusters with Tunable Components, Band Gaps, and Fluorescence Properties, *Dalton Trans.*, 2018, **47**, 5977–5984.

17 C. Zimmermann, M. Melullis and S. Dehnen, Reactivity of Chalcogenostannate Salts: Unusual Synthesis and Structure of a Compound Containing Ternary Cluster Anions $[Co_4(M_4\text{-}Se)(SnSe_4)_4]^{10-}$, *Angew. Chem., Int. Ed.*, 2002, **41**, 4269–4272.

18 S. Dehnen and M. K. Brandmayer, Reactivity of Chalcogenostannate Compounds: Syntheses, Crystal Structures, and Electronic Properties of Novel Compounds Containing Discrete Ternary Anions $[MII_4(M_4\text{-}Se)(SnSe_4)_4]^{10-}$ (MII = Zn, Mn), *J. Am. Chem. Soc.*, 2003, **125**, 6618–6619.

19 J. Zhang, C. Qin, Y. Zhong, X. Wang, W. Wang, D. Hu, X. Liu, C. Xue, R. Zhou, L. Shen, Y. Song, D. Xu, Z. Lin, J. Guo, H. Su, D.-S. Li and T. Wu, Atomically Precise Metal-Chalcogenide Semiconductor Molecular Nanoclusters with

High Dispersibility: Designed Synthesis and Intracluster Photocarrier Dynamics, *Nano Res.*, 2020, **2**, 2828–2836.

20 Y. Liu, Q. Lin, Q. Zhang, X. Bu and P. Feng, Visible-Light-Driven, Tunable, Photoelectrochemical Performance of a Series of Metal-Chelate, Dye-Organized, Crystalline, CdS Nanoclusters, *Chem. – Eur. J.*, 2014, **20**, 8297–8301.

21 C. Xu, N. Hedin, H.-T. Shi and Q.-F. Zhang, A Semiconducting Microporous Framework of $Cd_6Ag_4(Sph)_{16}$ Clusters Interlinked Using Rigid and Conjugated Bipyridines, *Chem. Commun.*, 2014, **50**, 3710–3712.

22 F. Kato and K. R. Kittilstved, Site-Specific Doping of Mn^{2+} in a CdS-Based Molecular Cluster, *Chem. Mater.*, 2018, **30**, 4720–4727.

23 X. Han, Z. Wang, D. Liu, J. Xu, Y. Liu and C. Wang, Co-Assembly of a Three-Dimensional Open Framework Sulfide with a Novel Linkage between an Oxygen-Encapsulated T3 Cluster and a Supertetrahedral T2 Cluster, *Chem. Commun.*, 2014, **50**, 796–798.

24 Q. Lin, X. Bu and P. Feng, An Infinite Square Lattice of Super-Supertetrahedral T6-Like Tin Oxyselenide Clusters, *Chem. Commun.*, 2014, **50**, 4044–4046.

25 X. Han, J. Xu, Z. Wang, D. Liu and C. Wang, A Hybrid Linkage Mode between T2,2 and T3 Selenide Clusters, *Chem. Commun.*, 2015, **51**, 3919–3922.

26 W. Wang, H. Yang, C. Xue, M. Luo, J. Lin, D. Hu, X. Wang, Z. Lin and T. Wu, The First Observation on Dual Self-Closed and Extended Assembly Modes in Supertetrahedral T3 Cluster Based Open-Framework Chalcogenide, *Cryst. Growth Des.*, 2017, **17**, 2936–2940.

27 J. Lv, W. Wang, L. Zhang, C. Xue, D. Hu and T. Wu, Assembly of Oxygen-Stuffed Supertetrahedral T3-Snos Clusters into Open Frameworks with Single Sn^{2+} Ion as Linker, *Cryst. Growth Des.*, 2018, **18**, 4834–4837.

28 T. Wu, F. Zuo, L. Wang, X. Bu, S.-T. Zheng, R. Ma and P. Feng, A Large Indium Sulfide Supertetrahedral Cluster Built from Integration of Zns-Like Tetrahedral Shell with Nacl-Like Octahedral Core, *J. Am. Chem. Soc.*, 2011, **133**, 15886–15889.

29 W. Wang, X. Wang, J. Zhang, H. Yang, M. Luo, C. Xue, Z. Lin and T. Wu, Three-Dimensional Superlattices Based on Unusual Chalcogenide Supertetrahedral in–Sn–S Nanoclusters, *Inorg. Chem.*, 2019, **58**, 31–34.

30 X. Zhang, Q. Wang, Z. Ma, J. He, Z. Wang, C. Zheng, J. Lin and F. Huang, Synthesis, Structure, Multiband Optical, and Electrical Conductive Properties of a 3d Open Cubic Framework Based on $[Cu_8Sn_6S_{24}]Z^-$ Clusters, *Inorg. Chem.*, 2015, **54**, 5301–5308.

31 H. Yang, L. Wang, D. Hu, J. Lin, L. Luo, H. Wang and T. Wu, A Novel Copper-Rich Open-Framework Chalcogenide Constructed from Octahedral Cu_4Se_6 and Icosahedral Cu_8Se_{13} Nanoclusters, *Chem. Commun.*, 2016, **52**, 4140–4143.

32 M. Luo, D. Hu, H. Yang, D. Li and T. Wu, Pcu-Type Copper-Rich Open-Framework Chalcogenides: Pushing up the Length Limit of the Connection Mode and the First Mixed-Metal $[Cu_7GeSe_{13}]$ Cluster, *Inorg. Chem. Front.*, 2017, **4**, 387–392.

33 R.-C. Zhang, J.-C. Zhang, Z. Cao, J.-J. Wang, S.-S. Liang, H.-J. Cong, H.-J. Wang, D.-J. Zhang and Y.-L. An, Unusual Flexibility of Microporous Sulfides During Ion Exchange, *Inorg. Chem.*, 2018, **57**, 13128–13136.

34 B. Han, J. Wang, Y. Liu, X. Wang, C. Xue, J. Lv, Z. Wu, R. Zhou, D. Xu, D.-S. Li and T. Wu, Two Copper-Rich Open-Framework Chalcogenides Built from Unusual $[Cu_5(Sn_xM_{1-x})Se_{10}]$ Clusters and $[(Sn_xM_{1-x})_2Se_6]$ Dimeric Linkers (M = In and Ga), *Inorg. Chem.*, 2020, **59**, 7919–7923.

35 Y. Lin, W. Massa and S. Dehnen, "Zeoball" $[Sn_{36}Ge_{24}Se_{132}]^{24-}$: A Molecular Anion with Zeolite-Related Composition and Spherical Shape, *J. Am. Chem. Soc.*, 2012, **134**, 4497–4500.

36 B. Seidlhofer, J. Djamil, C. Näther and W. Bensch, From Zero- to Three-Dimensional Thioantimonates: $[Ni(Aepa)_2]_3Sb_6S_{12}$ (Aepa = $C_5H_{15}N_3$ = N-(Aminoethyl)-1,3-Propandiamine), Containing the Unique $[Sb_6S_{12}]^{6-}$ Cyclic Anion, $[Ni(Aepa)_2]_6(Sb_3S_6)_2(SO_4)_3{\cdot}2H_2O$, with Isolated $[Sb_3S_6]^{3-}$ Anions and $[Ni(Aepa)_2]Sb_4S_7$, Characterized by a Three-Dimensional Network Structure, *Cryst. Growth Des.*, 2011, **11**, 5554–5560.

37 Y.-H. Wang, W. Luo, J.-B. Jiang, G.-Q. Bian, Q.-Y. Zhu and J. Dai, A Wheel-Shaped Indium–Telluride Nanocluster $[In_{18}Te_{30}(Dach)_6]^{6-}$: Its Formation and Structure, *Inorg. Chem.*, 2012, **51**, 1219–1221.

38 X. Zhang, Y.-Y. Pu, L.-S. You, G.-Q. Bian, Q.-Y. Zhu and J. Dai, Wheel-Shaped Indium Telluride Nanoclusters Co-Crystallized with Metal-Phenanthroline Complexes, *Polyhedron*, 2013, **52**, 645–649.

39 Y.-H. Wang, J. Wu, X.-W. Zhao, L.-W. Qian, Q.-Y. Zhu and J. Dai, A Nano-Scale Triangular Ring Cluster of Indium–Selenide: The Structure and Templating Effect, *Chem. Commun.*, 2015, **51**, 10668–10671.

40 C. Wang, X. Bu, N. Zheng and P. Feng, A 3D Open–Framework Indium Telluride and Its Selenide and Sulfide Analogues, *Angew. Chem., Int. Ed.*, 2002, **41**, 1959–1961.

41 N. Ding, D.-Y. Chung and M. G. Kanatzidis, $K_6Cd_4Sn_3Se_{13}$: A Polar Open-Framework Compound Based on the Partially Destroyed Supertetrahedral $[Cd_4Sn_4Se_{17}]^{10-}$ Cluster, *Chem. Commun.*, 2004, **10**, 1170–1171.

42 S. J. Ewing and P. Vaqueiro, Structural Complexity in Indium Selenides Prepared Using Bicyclic Amines as Structure-Directing Agents, *Dalton Trans.*, 2015, **44**, 1592–1600.

43 C. Xue, L. Zhang, X. Wang, X. Wang, J. Zhang and T. Wu, Highly Open Chalcogenide Frameworks Built from Unusual Defective Supertetrahedral Clusters, *Dalton Trans.*, 2019, **48**, 10799–10803.

44 M. G. Sorolla, X. Wang, T. Makarenko and A. J. Jacobson, A Large Spin, Magnetically Anisotropic, Octanuclear Vanadium(III) Wheel, *Chem. Commun.*, 2019, **55**, 342–344.

45 J. F. You, G. C. Papaefthymiou and R. H. Holm, [Beta-$Na_2Fe_{18}S_{30}]^{8-}$ and $[Na_9Fe_{20}Se_{38}]^{9-}$: High-Nuclearity Clusters by Mono- or Bicyclization of Unidimensional Polymeric Fragments and the Existence of Isomeric Monocyclic Clusters, *J. Am. Chem. Soc.*, 1992, **114**, 2697–2710.

46 J. F. You, B. S. Snyder and R. H. Holm, $[Na_2Fe_{18}S_{30}]^{8-}$. A High-Nuclearity Cyclic Cluster Generated Solely by Iron-Sulfur Bridge Bonding, *J. Am. Chem. Soc.*, 1988, **110**, 6589–6591.
47 P. King, T. C. Stamatatos, K. A. Abboud and G. Christou, Reversible Size Modification of Iron and Gallium Molecular Wheels: A Ga10 "Gallic Wheel" and Large Ga18 and Fe18 Wheels, *Angew. Chem., Int. Ed.*, 2006, **45**, 7379–7383.
48 E. C. Sañudo, C. A. Muryn, M. A. Helliwell, G. A. Timco, W. Wernsdorfer and R. E. P. Winpenny, Al, Ga and in Heterometallic Wheels and Their by-Products, *Chem. Commun.*, 2007, 801–803.
49 T. C. Stamatatos, S. Mukherjee, K. A. Abboud and G. Christou, The Largest Single-Strand Molecular Wheel: Ga_{20} from a Targeted, Diolate-Induced Size Modification of the Ga_{10}'Gallic Wheel', *Chem. Commun.*, 2009, 62–64.
50 D. Shi, X. Yang, H. Chen, D. Jiang, J. Liu, Y. Ma, D. Schipper and R. A. Jones, Large Ln_{42} Coordination Nanorings: Nir Luminescence Sensing of Metal Ions and Nitro Explosives, *Chem. Commun.*, 2019, **55**, 13116–13119.
51 L. Geng, C.-H. Liu, S.-T. Wang, W.-H. Fang and J. Zhang, Designable Aluminum Molecular Rings: Ring Expansion and Ligand Functionalization, *Angew. Chem., Int. Ed.*, 2020, **59**, 16735.
52 Q. Xu, B. Xu, H. Kong, P. He, J. Wang, T. Kannan, P. Ma, J. Wang and J. Niu, Synthesis and Characterization of a Crown-Shaped 36-Molybdate Cluster and Application in Catalyzing Knoevenagel Condensation, *Inorg. Chem.*, 2020, **59**, 10665–10672.
53 R. C. Maji, P. P. Das, A. Bhandari, S. Mishra, M. Maji, K. B. Ghiassi, M. M. Olmstead and A. K. Patra, Mixed Valence Copper–Sulfur Clusters of Highest Nuclearity: A Cu_8 Wheel and a Cu_{16} Nanoball, *Chem. Commun.*, 2017, **53**, 3334–3337.
54 X.-Y. Zheng, Y.-H. Jiang, G.-L. Zhuang, D.-P. Liu, H.-G. Liao, X.-J. Kong, L.-S. Long and L.-S. Zheng, A Gigantic Molecular Wheel of $\{Gd_{140}\}$: A New Member of the Molecular Wheel Family, *J. Am. Chem. Soc.*, 2017, **139**, 18178–18181.
55 J. Lin, N. Li, S. Yang, M. Jia, J. Liu, X.-M. Li, L. An, Q. Tian, L.-Z. Dong and Y.-Q. Lan, Self-Assembly of Giant Mo_{240} Hollow Opening Dodecahedra, *J. Am. Chem. Soc.*, 2020, **142**, 13982–13988.
56 Z. Wu, I. Nußbruch, S. Nier and S. Dehnen, Ionothermal Access to Defined Oligomers of Supertetrahedral Selenido Germanate Clusters, *JACS Au*, 2022, **2**, 204–213.
57 X. Bu, N. Zheng and P. Feng, Tetrahedral Chalcogenide Clusters and Open Frameworks, *Chem. – Eur. J.*, 2004, **10**, 3356–3362.
58 P. Feng, X. Bu and N. Zheng, The Interface Chemistry between Chalcogenide Clusters and Open Framework Chalcogenides, *Acc. Chem. Res.*, 2005, **38**, 293–303.
59 S. D. Nogai and H. Schmidbaur, Preparation and Structure of Soluble Complexes of the Ternary Compounds Gasbr and Gasebr, *Dalton Trans.*, 2003, 2488–2495.
60 P. Vaqueiro, M. L. Romero, B. C. Rowan and B. S. Richards, Arrays of Chiral Nanotubes and a Layered Coordination Polymer Containing Gallium–Sulfide Supertetrahedral Clusters, *Chem. – Eur. J.*, 2010, **16**, 4462–4465.
61 W.-W. Xiong, J.-R. Li, B. Hu, B. Tan, R.-F. Li and X.-Y. Huang, Largest Discrete Supertetrahedral Clusters Synthesized in Ionic Liquids, *Chem. Sci.*, 2012, **3**, 1200–1204.
62 Z.-Q. Li, C.-J. Mo, Y. Guo, N.-N. Xu, Q.-Y. Zhu and J. Dai, Discrete Supertetrahedral Cuins Nanoclusters and Their Application in Fabrication of Cluster-Sensitized Tio_2 Photoelectrodes, *J. Mater. Chem. A*, 2017, **5**, 8519–8525.
63 Y. Zhang, X. Wang, D. Hu, C. Xue, W. Wang, H. Yang, D. Li and T. Wu, Monodisperse Ultrasmall Manganese-Doped Multimetallic Oxysulfide Nanoparticles as Highly Efficient Oxygen Reduction Electrocatalyst, *ACS Appl. Mater. Interfaces*, 2018, **10**, 13413–13424.
64 D. Liu, X. Fan, X. Wang, D. Hu, C. Xue, Y. Liu, Y. Wang, X. Zhu, J. Guo, H. Lin, Y. Li, J. Zhong, D. Li, X. Bu, P. Feng and T. Wu, Cooperativity by Multi-Metals Confined in Supertetrahedral Sulfide Nanoclusters to Enhance Electrocatalytic Hydrogen Evolution, *Chem. Mater.*, 2019, **31**, 553–559.
65 C. Xue, L. Zhang, X. Wang, D. Hu, X.-L. Wang, J. Zhang, R. Zhou, D.-S. Li, H. Su and T. Wu, Enhanced Water Dispersibility of Discrete Chalcogenide Nanoclusters with a Sodalite-Net Loose-Packing Pattern in a Crystal Lattice, *Inorg. Chem.*, 2020, **59**, 15587–15594.
66 M.-B. Luo, S.-L. Huang, H.-D. Lai, J. Zhang and Q. Lin, Tin-Oxychalcogenide Supertetrahedral Clusters Maintained in a Mtn Zeolite-Analog Arrangement by Coulombic Interactions, *Chem. Commun.*, 2020, **56**, 8388–8391.
67 J. Lin, Y. Dong, Q. Zhang, D. Hu, N. Li, L. Wang, Y. Liu and T. Wu, Interrupted Chalcogenide-Based Zeolite-Analogue Semiconductor: Atomically Precise Doping for Tunable Electro-/Photoelectrochemical Properties, *Angew. Chem., Int. Ed.*, 2015, **54**, 5103–5107.
68 S.-L. Huang, L. He, E.-X. Chen, H.-D. Lai, J. Zhang and Q. Lin, A Wide Ph-Range Stable Crystalline Framework Based on the Largest Tin-Oxysulfide Cluster $[Sn_{20}O_{10}S_{34}]$, *Chem. Commun.*, 2019, **55**, 11083–11086.
69 L. Nie and Q. Zhang, Recent Progress in Crystalline Metal Chalcogenides as Efficient Photocatalysts for Organic Pollutant Degradation, *Inorg. Chem. Front.*, 2017, **4**, 1953–1962.
70 H. Pei and L. Wang, An Open Framework Chalcogenide Supertetrahedral Cluster as Visible-Light Driven Photocatalysts for Selective Degradation, *Cryst. Growth Des.*, 2019, **19**, 5716–5719.
71 H. Pei, L. Wang and M.-H. Zeng, Selectively Photocatalytic Activity of an Open-Framework Chalcogenide Built from Corner-Sharing T4 Supertetrahedral Clusters, *Inorg. Chem.*, 2019, **58**, 12011–12016.
72 C.-Y. Yue, Y.-D. Yue, H.-X. Sun, D.-Y. Li, N. Lin, X.-M. Wang, Y.-X. Jin, Y.-H. Dong, Z.-H. Jing and X.-W. Lei, Transition Metal Complex Dye-Sensitized 3d Iodoplumbates: Syntheses, Structures and Photoelectric Properties, *Chem. Commun.*, 2019, **55**, 6874–6877.

73 H. Wang, Y. Wu, M. Feng, W. Tu, T. Xiao, T. Xiong, H. Ang, X. Yuan and J. W. Chew, Visible-Light-Driven Removal of Tetracycline Antibiotics and Reclamation of Hydrogen Energy from Natural Water Matrices and Wastewater by Polymeric Carbon Nitride Foam, *Water Res.*, 2018, **144**, 215–225.

74 H. Wang, X. Yuan, Y. Wu, G. Zeng, X. Chen, L. Leng and H. Li, Synthesis and Applications of Novel Graphitic Carbon Nitride/Metal-Organic Frameworks Mesoporous Photocatalyst for Dyes Removal, *Appl. Catal., B*, 2015, **174–175**, 445–454.

75 Y. Yan, M. Zhang, K. Gong, L. Su, Z. Guo and L. Mao, Adsorption of Methylene Blue Dye onto Carbon Nanotubes: A Route to an Electrochemically Functional Nanostructure and Its Layer-by-Layer Assembled Nanocomposite, *Chem. Mater.*, 2005, **17**, 3457–3463.

76 Z. Wu, X.-L. Wang, X. Wang, X. Xu, D.-S. Li and T. Wu, 0D/2D Heterostructure Constructed by Ultra-Small Chalcogenide-Cluster Aggregated Quaternary Sulfides and g-C_3N_4 for Enhanced Photocatalytic H_2 Evolution, *Chem. Eng. J.*, 2021, **426**, 131216.